ANALYSIS OF ENDOSOMAL SORTING COMPLEX REQUIRED FOR TRANSPORT-III PROTEIN FUNCTIONS IN THE ABSCISSION STEP OF CYTOKINESIS

by

Brandon W. Henrie

A thesis submitted to the faculty of
The University of Utah
in partial fulfillment of the requirements for the degree of

Master of Science

Department of Biochemistry

The University of Utah

December 2013

ProQuest LLC.
789 East Eisenhower Parkway
P.O. Box 1346
Ann Arbor, MI 48106 - 1346

The University of Utah Graduate School

STATEMENT OF THESIS APPROVAL

The thesis of **Brandon W. Henrie**

has been approved by the following supervisory committee members:

Wesley I. Sundquist	, Chair	**July 31, 2013** Date Approved
Adam Frost	, Member	**July 31, 2013** Date Approved
Katie Ullman	, Member	**July 31, 2013** Date Approved

and by **Wesley I. Sundquist** , Chair/Dean of

the Department/College/School of **Biochemistry**

and by David B. Kieda, Dean of The Graduate School.

ABSTRACT

The mammalian Endosomal Sorting Complex Required for Transport (ESCRT) pathway mediates the final membrane fission step of cytokinesis, known as abscission. Prior to abscission, the ESCRT machinery is recruited to the intercellular bridge that connects nascent daughter cells. Once there, subunits of the ESCRT-III complex bind the plasma membrane and oligomerize into membrane-bound filaments. These filaments constrict the membrane, resulting in membrane fission and release of two independent daughter cells.

Here, I describe the creation of siRNA/shRNA depletion and rescue assays for testing abscission functions of the ESCRT-III proteins IST1 and CHMP2A. siRNA or shRNA treatments were used to deplete endogenous IST1 or CHMP2A protein levels, and exogenous wild-type or mutant constructs were tested for their ability to “rescue” the resulting abscission defects, as assayed by flow cytometry or morphological assays. These assays confirmed that both IST1 and CHMP2A are required for abscission, and that exogenous wild-type IST1 and CHMP2A can rescue the defects induced by depletion of the cognate proteins.

The IST1 and CHMP2A depletion/rescue assays provided a means for testing whether different IST1 and CHMP2A mutants can function in abscission. As an initial proof of principle, I tested whether mutations in conserved basic

patches in the N-terminal alpha helix inhibit the ability of IST1 and CHMP2A to function in abscission. Tests were performed because previous studies had implicated these basic patches in ESCRT-III membrane binding. Consistent with this hypothesis, mutations in the basic residues of IST1 abolished abscission functions; however, the CHMP2A data were ambiguous. Thus, my work has confirmed that the ESCRT-III proteins IST1 and CHMP2A are both required for the abscission step of cytokinesis, and have provided an assay system that can be used to test the functionality of mutant proteins.

TABLE OF CONTENTS

LIST OF FIGURES

CHAPTER 1

INTRODUCTION

Overview of the ESCRT Pathway

The Endosomal Sorting Complexes Required for Transport (ESCRT) pathway mediates membrane fission events in a variety of cellular processes including: multivesicular bodies (MVB) vesicle formation, shedding microvesicle formation, exosome formation, and abscission (the final membrane fission event in cytokinesis)[1]. This pathway is also required for the budding of enveloped viruses such as HIV, arenaviruses, filoviruses, paramyxoviruses, orbiviruses, and rhabdoviruses[2,3,4].

These are all "reverse topology" membrane fission events in which the membrane is constricted *towards* the cytoplasm by ESCRT proteins that act *within* the membrane tube where fission will take place (Fig. 1.1). Conversely, in "normal topology" membrane fission events, the membrane is constricted *towards* the extracellular space by proteins that act from the *outside* of the membrane tube (*e.g.*, as in endocytosis and COP-I and COP-II-mediated vesicle formation; Fig. 1.1) [5,6].

The ESCRT pathway was discovered through yeast genetic screens designed to identify proteins required for proper vacuole protein sorting (*vps*)[7]. The yeast vacuole (lysosome in animal cells) plays a central role in a series in physiological processes such as osmoregulation, amino acid storage, and protein degradation[1,7]. Membrane proteins targeted for degradation are typically first sorted into vesicles that bud into the lumen of MVBs[1]. These proteins are delivered for degradation when the MVB fuses with the vacuole. The original yeast vacuole protein sorting mutant strains were divided into six classes

(classes A–F) based on the morphologies of their vacuoles[8]. The class E *vps* mutants were subsequently further divided into five multiprotein complexes termed ESCRT-0, -I, -II, -III, and Vps4[9,10,11,12]. ESCRT-0 is now considered to be an endosome-specific ESCRT adaptor, and the ESCRT-I, -II, -III, and VPS4 complexes, together with Bro1 protein family members, constitute the core ESCRT pathway components[2].

Recruitment of the ESCRT Pathway

The core complexes of the ESCRT pathway are recruited sequentially to sites of membrane fission. ESCRT pathway recruitment can be subdivided into three stages: first, adaptor proteins like ESCRT-0 mark a future site of membrane fission; second, early-acting ESCRT factors ALIX, ESCRT-I, and ESCRT-II arrive and stabilize the vesicle neck; third, the late-acting ESCRT factors ESCRT-III and VPS4 arrive and catalyze membrane fission. Each of these different stages is discussed below in greater detail.

Process-specific adaptor proteins initiate ESCRT recruitment to different sites of action. Examples of adaptor proteins include: ESCRT-0 (*e.g.*, HRS:STAM and related endosomal adaptors, MVB formation), ARRDC1 (shedding microvesicle formation), Gag (retrovirus budding), and CEP55 (abscission)[13,14,15,16,17,18]. Adaptor proteins are localized to their specific sites of action through adaptor:membrane and adaptor:protein interactions[19,20].

The early-acting factors of the ESCRT pathway are then recruited to a site of action by direct binding to process-specific adaptor proteins. The early-acting

ESCRT factors include: the ESCRT-I/ESCRT-II supercomplex, and Bro1 protein family members (*i.e.*, proteins such as ALIX that contain a Bro1 domain)[2].

The late-acting factors of the ESCRT pathway, ESCRT-III and VPS4, bind directly to the early-acting factors[2]. Unlike the other discrete ESCRT complexes, subunits of the ESCRT-III complex do not bind one another until they coassemble on the membrane with the exception of IST1 and CHMP1B, which form a binary complex in yeast[21,22,23]. Humans express a total of 12 ESCRT-III proteins that comprise 8 families (termed Charged Multivesicular Body Proteins) CHMP1–7 and Increased Sodium Tolerance 1 (IST1), with three different CHMP4 proteins (A, B, and C) and two different CHMP1 (A, B) and CHMP2 (A, B) proteins; Fig. 1.2a). All ESCRT-III proteins share a conserved core structure known as the ESCRT-III fold, which is made up of four alpha helices[24,25]. Helices one and two form a helical hairpin, and helices three and four pack against the open end of the hairpin (Fig. 1.2b). The ESCRT-I/-II supercomplex binds directly to CHMP6, and the Bro domains of Bro1 protein family members such as ALIX, BROX, and HD-PTP bind directly to CHMP4 and CHMP5 proteins[26,27,28,29,30,31]. The different ESCRT-III proteins are thought to copolymerize into membrane-associated filaments[32,33,34,35]. The VPS4 ATPase then binds to different sites on the exposed C-terminal tails of the polymerized ESCRT-III filaments, thereby completing ESCRT factor recruitment[36,37,38]. VPS4 provides the energy for ESCRT-III-mediated membrane fission by using ATP hydrolysis to disassemble ESCRT-III filaments and may also participate directly in the fission reaction[32,39,40,41,42].

Models for ESCRT-III Mediated Membrane Fission

It is not yet clear how ESCRT-III filaments and VPS4 accomplish membrane fission, but three general models have been proposed: the dome model, the break and slide model, and the whorl model (Fig. 1.3)[42,43,44,45]. These models all incorporate direct involvement of membrane-bound ESCRT-III filaments and postulate a role for VPS4. According to the dome model (Fig. 1.3a), ESCRT-III filaments spiral into a helical dome, which binds and constricts to a point[43]. VPS4 then disassembles the ESCRT-III filaments to recycle their constituent subunits. In the break and slide model (Fig. 1.3b, proposed only for the abscission step of cytokinesis), ESCRT-III filaments initially form wide helices approximately one micron away from the eventual membrane fission site[42,44]. VPS4 then severs the ESCRT-III helices and the distal part constricts by twisting, relocalizes to a narrower site, and then forms a dome that mediates membrane fission. In the whorl model (Fig. 1.3c, proposed to explain MVB vesicle formation), multiple ESCRT-I/ESCRT-II supercomplexes deform the membrane and stabilize the vesicle neck[45]. These ESCRT-I/ESCRT-II supercomplexes also nucleate the formation of 6–10 ESCRT-III filaments, which then grow into the center of the lumen of the vesicle neck forming a “whorl” that draws the membrane inward to a fission point.

The Abscission Step of Cytokinesis

The ESCRT pathway mediates the abscission step of cytokinesis[17,46,47]. Cytokinesis begins during the mitotic phase of the cell cycle and progresses

through ingression of the cleavage furrow until the nascent daughter cells are connected by a narrow membrane tube (the intercellular bridge). The abscission event then separates the bridge to produce two discrete daughters.

The cell cycle is the series of events that ultimately leads to the duplication of a parent cell to produce two independent daughters (Fig. 1.4). Mitosis is the cell cycle phase in which a cell segregates its DNA into the nascent daughters (Fig. 1.4). During the metaphase stage of mitosis, sister chromosomes attached to microtubules align on the equatorial metaphase plate, forming a bipolar spindle (Fig. 1.5). The aligned sister chromosomes are then pulled toward the poles at the onset of anaphase. The spindle microtubule organization provides the spatial and temporal cues for the formation of an equatorial ring of myosin II and actin known as a contractile ring (Fig. 1.5)[48,49]. Contractile ring formation marks the beginning of cytokinesis.

The contractile ring constricts inward, creating a cleavage furrow (Fig. 1.5). Myosin II motor activity along the actin filaments of the contractile ring provides the force required for ingression of the furrow (Fig. 1.5)[50]. Contraction continues until the microtubules are compacted within a narrow intercellular bridge that connects the nascent daughter cells[51]. At the center of this bridge is a dark zone (known as a “Flemming Body” or “midbody”), which helps to organize the proteins involved in abscission[50,51].

The ESCRT pathway mediates the final membrane fission event of abscission by forming cut sites on one or both sides of the midbody. The adaptor protein CEP55 is recruited to the midbody of the intercellular bridge by the

microtubule interacting protein Centralspindlin[19]. CEP55 then recruits the early-acting factors of the ESCRT pathway, ALIX and ESCRT-I, which in turn bind and organize ESCRT-III proteins (Fig. 1.6) [18,25,26,28,29,46,52,53,54,55]. The ESCRT-III proteins form membrane-bound filaments and recruit VPS4 to complete abscission[17,25,56,57]. If ESCRT pathway recruitment is disrupted, then the cell arrests at the intercellular bridge stage, and the bridge can eventually coalesce back to reform a single, multinucleate cell (termed abscission failure)[56].

Many ESCRT-III Proteins are Required for Abscission

Most of the different human ESCRT-III proteins apparently play a role in abscission, although their functions are not fully understood. Depletion of the ESCRT-III proteins IST1, CHMP2A, or CHMP3 produces strong abscission failure[25,56,57]. CHMP1A, CHMP2B, CHMP4B, CHMP4C, and CHMP7 are also required for efficient abscission, although their depletion can also induce upstream mitotic defects[56]. Thus, depletion studies have established that IST1, CHMP2A, and CHMP3 are definitely required for abscission, and that most other ESCRT-III proteins probably are as well, although their abscission functions can be masked by mitotic defects under some conditions.

Rescue Assays For Analyses of ESCRT-III Abscission Functions

SiRNA or shRNA depletion and rescue assays (termed depletion/rescue assays) are increasingly used to test the proposed functions of proteins in

mammalian cell processes[58]. In these experiments, endogenous protein levels are lowered by siRNA or shRNA treatments, and an siRNA/shRNA-resistant exogenous protein is reintroduced and tested for phenotypic rescue. In cases where the wild-type, exogenous protein can functionally replace the endogenous protein, then mutant exogenous proteins can also be tested for function. Thus, a depletion/rescue assay is a powerful genetic approach for testing the functional importance of different protein elements in mammalian cells.

In my thesis research, I developed and tested depletion/rescue assays for the ESCRT-III proteins, IST1 and CHMP2A. In the next chapter, I show that exogenous, wild-type IST1 or CHMP2A can functionally replace the abscission functions of cognate endogenous IST1 or CHMP2A activities. I show that these assays can be used to test the functional importance of conserved basic patches on the ESCRT-III core that have been proposed to be the ESCRT-III membrane-binding surface.

In the future, I anticipate that analogous IST1 and CHMP2A depletion/rescue assays will allow researchers to dissect other mechanistic details of ESCRT-III function in abscission. Details of interest include: the structure of ESCRT-III monomers within ESCRT-III filaments and the protein:protein interactions within the membrane-bound filaments.

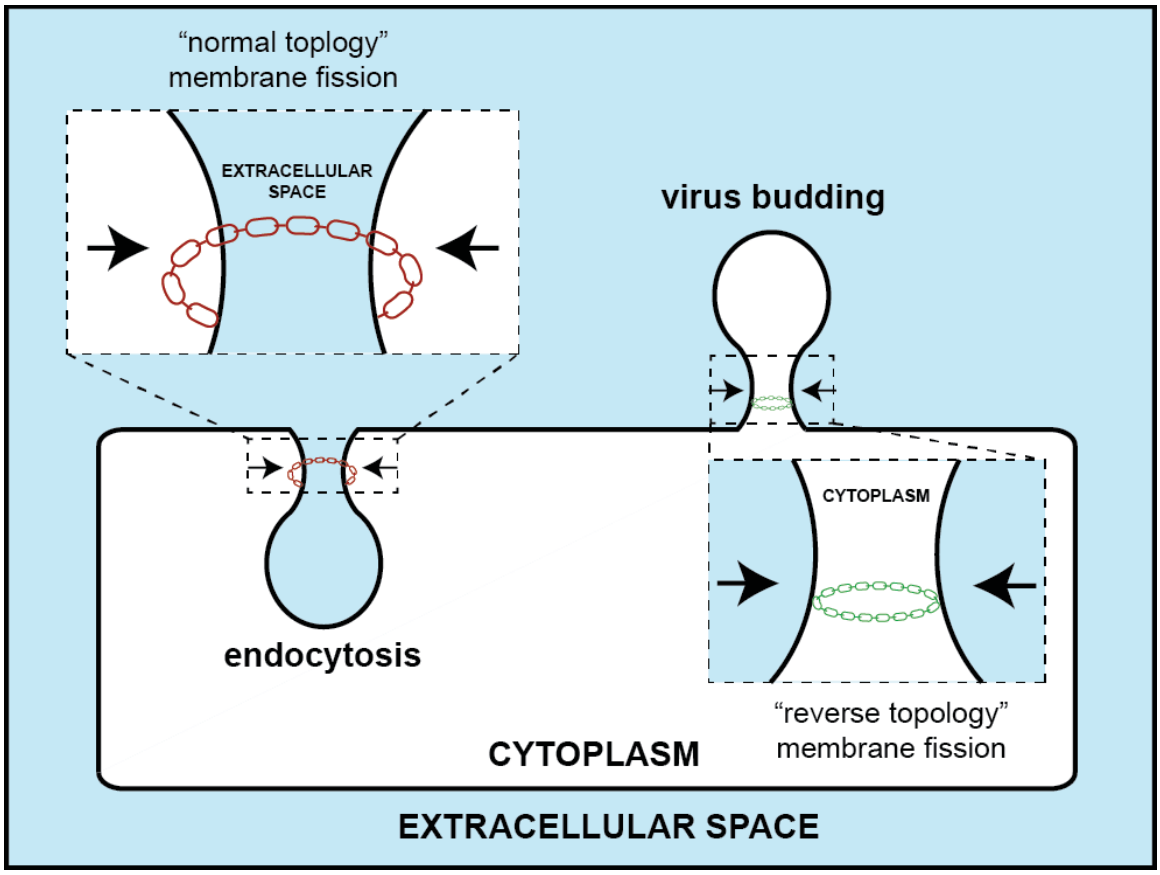

Figure 1.1: Membrane fission topologies. In "normal topology" membrane fission events such as endocytosis, the fission machinery (depicted schematically in red) is located on the outside of the vesicle neck and constricts the membrane towards the extracellular space. In "reverse topology" membrane fission events such as enveloped virus budding, the fission machinery (depicted schematically in green) is located within the bud neck and constricts the membrane towards the cytoplasm

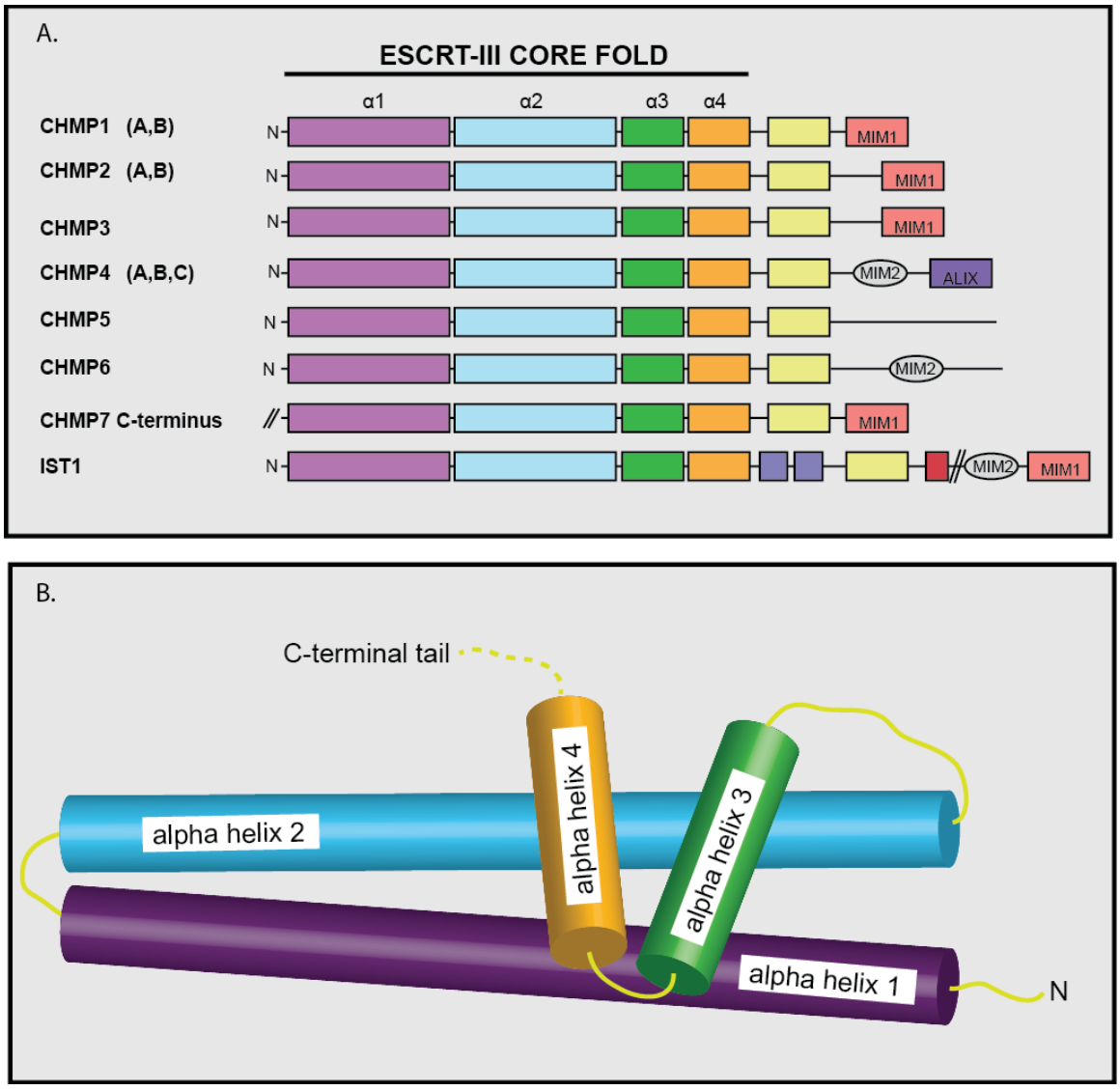

Figure 1.2: ESCRT-III proteins and the core ESCRT-III fold. (A) The 8 human ESCRT-III protein families. The names of the 12 human ESCRT-III proteins are given at the left and schematic illustrations of their constituent helices and factor binding sites are given at the right. Abbreviations: MIM1 (Type 1 MIT Interaction Motif), a VPS4 binding site; MIM2 (Type 2 MIT Interaction Motif), a VPS4 binding site; ALIX, ALIX protein binding site. Colored boxes denote helices. (B) Schematic diagram of the core ESCRT-III fold. Alpha helix 1 and alpha helix 2 form an extended hairpin and helices 3 and 4 pack against the open end of the hairpin. The color coding of the core helices matches that in part (A).

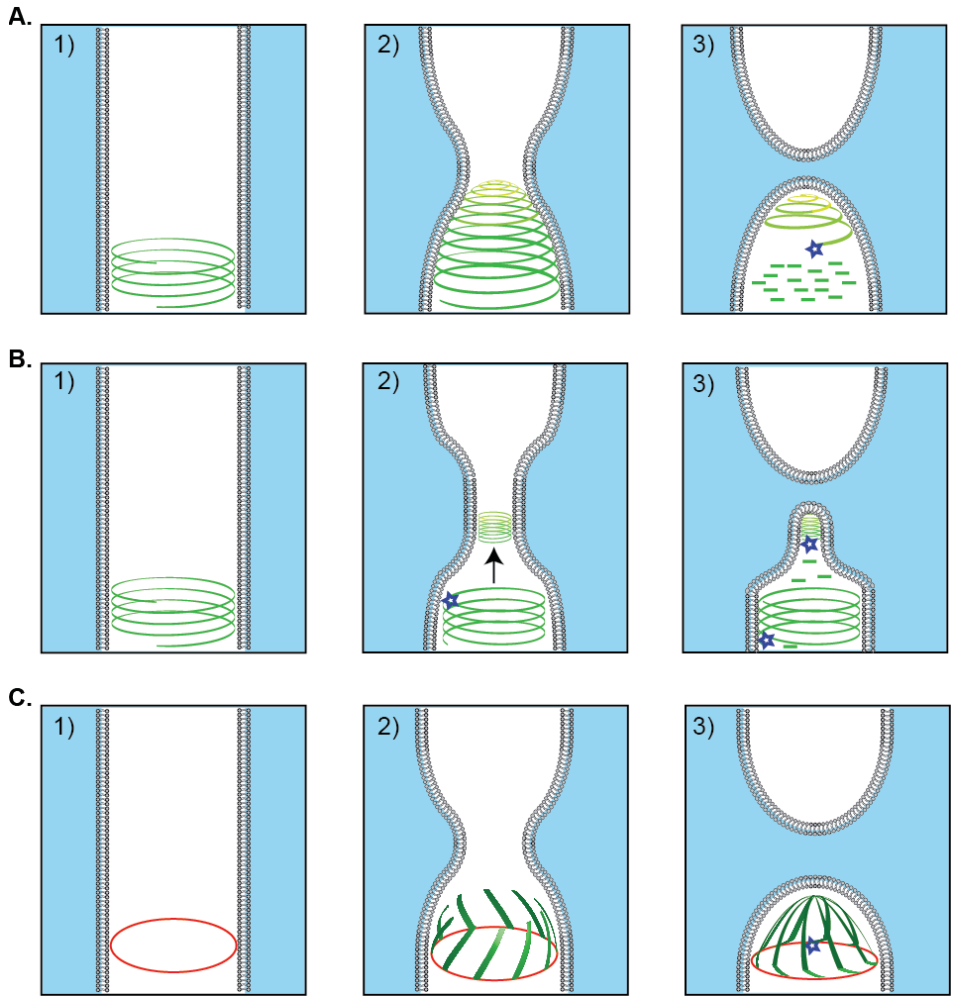

Figure 1.3: Models for ESCRT-mediated membrane fission. (A) Image representing the "dome model." 1) ESCRT-III filaments form helices at the base of the bud neck. 2) ESCRT-III filaments form constricting spirals that draw the associated membrane inward. 3) Membrane fission occurs at the apex of the ESCRT-III dome, and VPS4 (blue star) disassembles the ESCRT-III filaments. (B) Image representing the "break and slide model." 1) ESCRT-III filaments form helices at the base that initially have a wider diameter than the ground state helix. 2) VPS4 severs the ESCRT-III helices, which then constrict and localize to a narrower membrane site. 3) The relocalized ESCRT-III helix forms a dome that mediates membrane fission. VPS4 then disassembles the ESCRT-III filaments. (C) Image representing the "whorl model." 1) Multiple copies of the ESCRT-I and -II supercomplex localize to the bud neck (red circle). 2) The ESCRT-I and -II supercomplexes nucleate ESCRT-III filaments that grow toward the center of the bud neck. 3) The ESCRT-III filaments form a whorl pulling the membrane inward toward a fission point. VPS4 may be required to stabilize the fission point and then disassemble the ESCRT-III filaments.

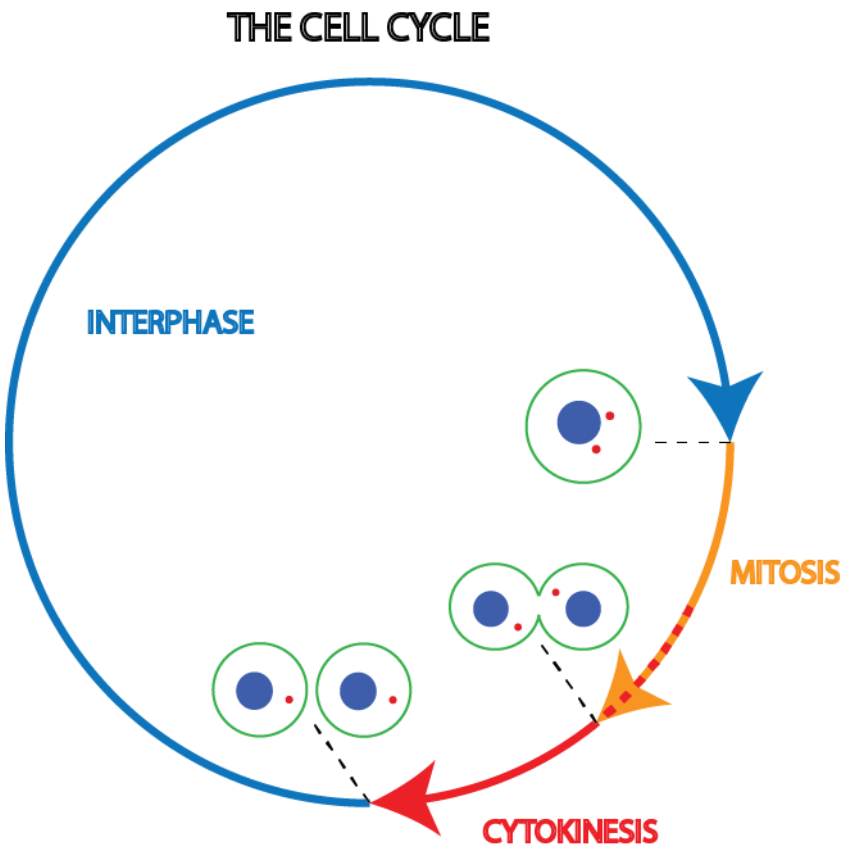

Figure 1.4: Overview of the cell cycle. In interphase, the cell duplicates its DNA, performs its cellular functions, and prepares for mitosis. In the mitotic phase, a cell segregates the sister chromatids to nascent daughter cells. In cytokinesis, the continuous membrane is divided, creating two independent daughter cells.

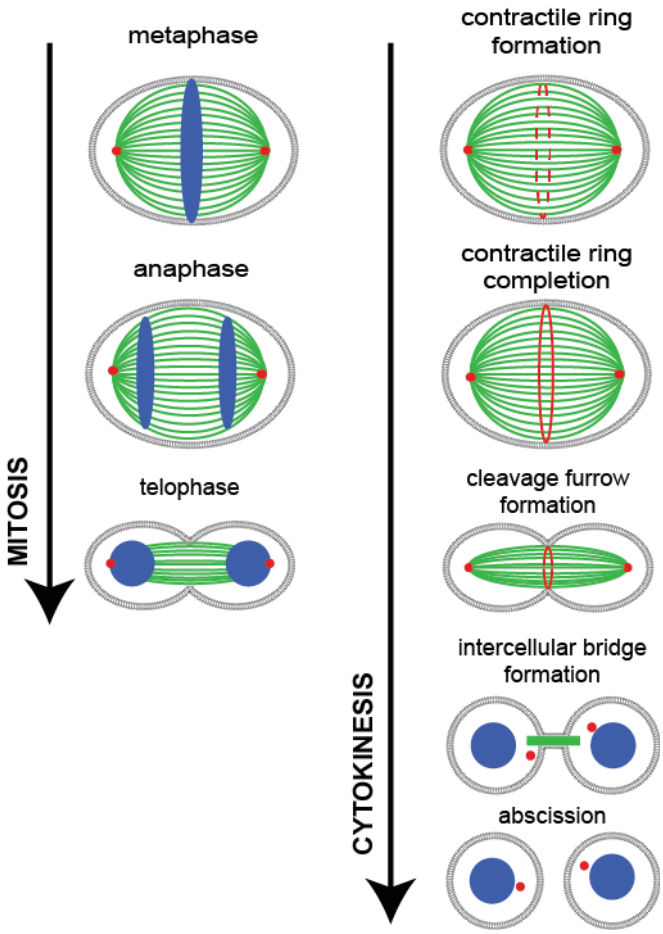

Figure 1.5: The timing and progression of cytokinesis. Between the start of metaphase and the end of anaphase the spindle microtubule organization provides the spatial and temporal cues necessary for formation of an equatorial contractile ring. The contractile ring ingresses to form a cleavage furrow during telophase and ultimately compacts the microtubules into a narrow intercellular bridge. Abscission then occurs producing two daughter cells.

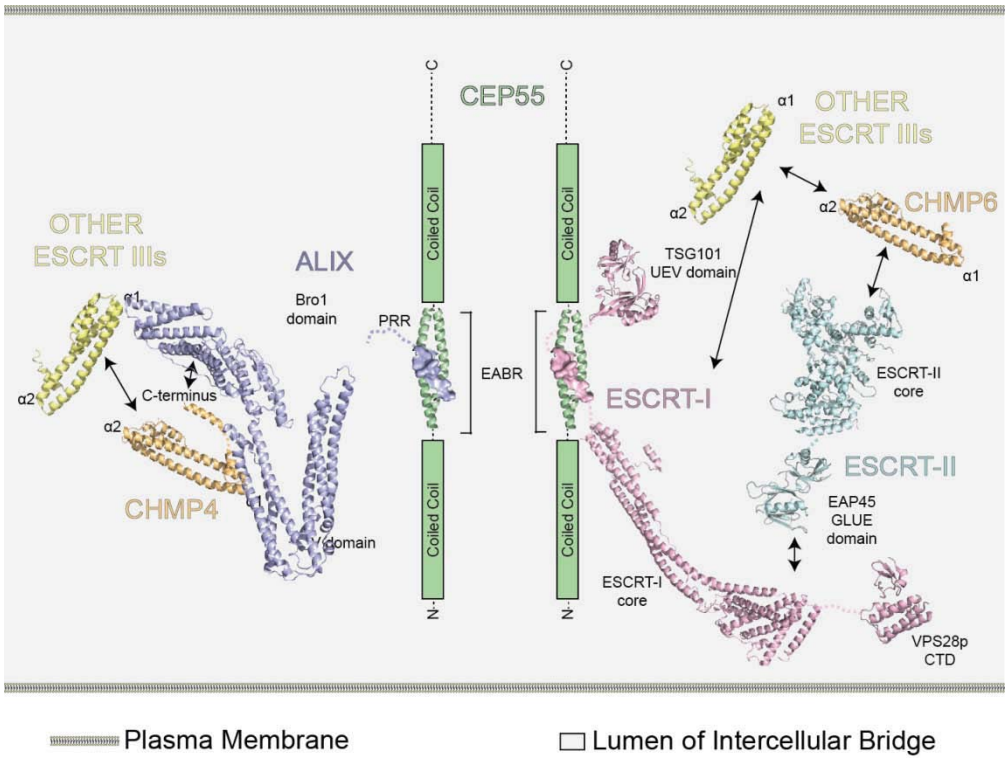

Figure 1.6: Organization of the ESCRT pathway during abscission. The adaptor protein, CEP55 (green), localizes to either edge of the midbody. CEP55 binds ALIX (purple) or the TSG101 subunit of ESCRT-I (pink) using a noncanonical coiled coil domain known as the ESCRT- and ALIX-binding region (EABR). The left half of the figure shows how ALIX then binds the C-terminal tail of CHMP4 (orange), which in turn interacts with other ESCRT-III proteins (yellow). The right half of the figure shows that ESCRT-I can form a super complex with ESCRT-II (teal). ESCRT-II binds the ESCRT-III protein CHMP6 (orange), which can bind CHMP4 proteins, leading to recruitment of other ESCRT-III proteins. The PDB accession numbers of the structures used to make this figure: 2OEV (ALIX), 2P22 (ESCRT-I), 1S1Q (TSG101 UEV), 2J9U (VPS28p CTD), 2ZME (ESCRT-II core), 2HTH (EAP45 GLUE domain), 3E1R (CEP55 EABR bound to PRR), and 2GD5 (CHMP3 used to represent the CHMP5 and CHMP4 cores). A CHMP2A homology model created using the PHYRE protein fold recognition server (http://www.sbg.bio.ic.ac.uk/~phyre/) was used to represent the core of other ESCRT-III proteins (*provided by Heidi Schubert*).

CHAPTER 2

ASSAYS FOR ESCRT-III FUNCTIONS IN ABSCISSION

Introduction

Abstract

The ESCRT pathway mediates "reverse topology" membrane fission events in a series of different cellular and viral processes including: enveloped virus budding, MVB vesicle formation, shedding microvesicle formation, exosome formation, and abscission (the final membrane fission event in cytokinesis)[2]. The ESCRT-I, -II, -III, VPS4 complexes, and Bro1 family proteins make up the core machinery of the ESCRT pathway. Fission is apparently affected by membrane-bound ESCRT-III filaments, which deform the membrane towards the cytoplasm ("reverse topology") ultimately leading to fission[32,33,34,59,60,61]. However, the mechanistic details of this process are unknown.

In this chapter, I describe the development and validation of depletion/rescue assays for IST1 and CHMP2A in abscission. These assays confirm that IST1 and CHMP2A are required in abscission. I also applied these assays to demonstrate the functional importance in abscission of basic patches on the N-terminal alpha helix of IST1 and CHMP2A. Thus, the IST1 and CHMP2A depletion/rescue assays can be used to test the functionality of mutant IST1 and CHMP2A proteins.

Rationale for IST1 studies

I chose IST1 as a target for depletion/rescue assay development for four reasons. First, IST1 is a strong effector of abscission; second, IST1 is likely directly involved in abscission; third, a high-resolution crystal structure of IST1 is

available, and electron microscopy (EM) reconstructions of IST1-containing filaments are forthcoming; and fourth, IST1 oliogmers can deform membranes *in vitro*, but the mechanisms underlying membrane constriction and fission by ESCRT-III filaments are not yet well understood.

Depletion of IST1 from HeLa cells induces abscission failure (an increase in the number of cells with an intercellular bridge and multinucleate cells as compared to a wild-type control), and the phenotype has a higher penetrance than the defects induced by depletion of other ESCRT-III proteins[25,56,57]. Thus, IST1 is a strong effector of abscission. A direct role for IST1 in abscission is supported by the observation that IST1 localizes to the intercellular bridge during cytokinesis. As shown in Fig. 2.1a, confocal fluorescence microscopy images of HeLa cells stained with an anti-IST1 antibody show strong IST1 localization (red) to the intercellular bridge during cytokinesis[25,57]. Super-resolution IST1 fluorescence images reveal that IST1 initially organizes into two rings, one on either side of the midbody (Fig. 2.1b upper panels). One or both of the rings then extrude and constrict to form continuous cones that narrow to the point of membrane fission (Fig. 2.1b lower panels). Thus, IST1 localizes to the intercellular bridge and forms structures that could constrict the plasma membrane to a fission point.

A high-resolution IST1 crystal structure and forthcoming IST1 filament structural studies make IST1 an attractive target for further functional characterization. The 1.8 angstrom resolution IST1 N-terminal domain ($IST1_{NTD}$, residues 1–189) crystal structure provides a detailed view of the core IST1

structural elements[23]. $IST1_{NTD}$ forms filaments *in vitro*, and ongoing studies are attempting to reconstruct the structure of the $IST1_{NTD}$:CHMP1B copolymer by EM (A. Frost and J. McCullough, personal communication)[23]. IST1 filaments can also deform lipid bilayers *in vitro*. As shown in Fig. 2.2A, purified $IST1_{NTD}$ filaments can organize into helical tubes that can extrude from the lumens of liposomes. These tubes appear to be capped by a "dome" of $IST1_{NTD}$ protein (Fig. 2.2a–c). Under these same conditions, $IST1_{NTD}$ filaments can also form spirals and/or concentric circles (Fig. 2.2d, e). These observations demonstrate that IST1 filaments can bind and deform lipids, and that the IST1 assemblies can narrow to form a dome providing a possible mechanistic explanation for IST1 function in abscission.

Rationale for CHMP2A studies

To extend my IST1 studies to other ESCRT-III proteins, I also developed a CHMP2A depletion/rescue assay. I chose CHMP2A because this protein, like IST1, is a strong effector of abscission, is likely directly involved in abscission, and because CHMP2A can form filaments and tubes *in vitro.*

SiRNA depletion experiments have established that CHMP2A is also required for abscission in HeLa cells[56]. The severity of the abscission failure induced by CHMP2A depletion is again greater than the defects induced by depletion of other ESCRT-III proteins, implying that CHMP2A is another strong abscission effector[56]. CHMP2A also forms rings and cones within the

intercellular bridge during cytokinesis. Thus, CHMP2A is also likely directly involved in abscission.

Finally, when co-incubated with CHMP3, CHMP2A lacking its C-terminus (CHMP2AΔC, residues 1-150) oilogmerizes into filaments, which wind up into helical tubes[32,33]. The similarities between CHMP2AΔC:CHMP3 and $IST1_{NTD}$:CHMP1B helical tubes suggests that CHMP2A and IST1 may perform analogous functions in abscission.

Validating the IST1 and CHMP2A rescue assays

Depletion/rescue experiments have proven to be a powerful approach for genetic analyses of protein functions in human cells[58]. These assays have two parts. First, siRNA/shRNA depletion of an endogenous protein must be shown to have a measureable phenotype. Second, reintroduction of the exogenous protein from an siRNA/shRNA resistant expression construct must be shown to rescue the phenotype. In this study, I demonstrate that silencing of either endogenous IST1 or CHMP2A results in strong abscission failure, and that reintroduction of exogenous IST1 and CHMP2A rescues the cognate phenotype.

Testing a model for ESCRT-III membrane binding

The crystal structure of CHMP3 revealed a large patch of basic residues on the first alpha helix that faces away from the core ESCRT-III domain[24]. Weissenhorn and colleagues have proposed that this conserved basic patch constitutes a phospholipid membrane binding surface[24]. Support for their model

comes from studies of CHMP3 membrane binding in enveloped virus budding. Specifically, they found that overexpressing GFP-PK-CHMP3ΔC (GFP-pyruvate kinase chimera, residues 1–150 of CHMP3) dominantly inhibited HIV-1 budding and resulted in accumulation of the CHMP3 fusion protein at the plasma membrane[24]. However, a mutant GFP-PK-CHMP3ΔC (R24S, K25A, R28S, R32A, and R35S) protein that lacked the basic patch failed to accumulate at the plasma membrane or to inhibit HIV-1 budding [24]. These results support a model in which the basic patch on the first alpha helix of ESCRT-III proteins mediates membrane binding. However, this model has not been rigorously tested, particularly in abscission.

I therefore performed depletion/rescue experiments, both to test the membrane binding model proposed by Weissenhorn and to confirm that my depletion/rescue assays can be used to test the functionality of IST1 and CHMP2A mutants in abscission[24]. To perform these studies, I generated siRNA/shRNA resistant constructs that expressed mutant IST1 and CHMP2A proteins lacking the basic patches and tested their ability to rescue abscission failure induced by depletion of the endogenous proteins.

Materials and Methods

Cell cultures

HeLa and 293T cells were grown in complete media (DMEM supplemented with 10% FBS and 2 mM L-glutamine) at 37º C with 5% CO_2.

PEI transfections

Prior to transfection, 293T cells were seeded at an initial density of $2x10^6$ cells/well in a 10 cm dish and allowed to grow for 24 h. Polyethylenimine (PEI, Polysciences 24765, final concentration of 0.82 μg/μl) was added along with DNA (12–15 μg) to 0.5 ml of complete media, and the solution was mixed by inverting the tube that was allowed to stand for 10 min at room temperature. The mixture was then added drop wise to the previously seeded 293T cells. The media was changed 12 h posttransfection, and the cells were harvested at the designated time points.

Expression vectors

ESCRT-III, HIV, MuLV, and control expression vectors used in this study are listed in Table 2.1.

Mutagenesis

The mutant YFP-IST1 3M construct (which expresses an IST1 protein with the following mutations: R16E, R27E, and K38E) was generated by replacing the SacI/AflII restriction digest fragment of the parental YFP-IST1 expression vector with a synthetic oligonucleotide that encoded the mutations.

The CHMP2A 3M construct was generated using a splicing by overlap extension PCR reaction (SOEing PCR). Briefly, a synthetic oligonucleotide matching the N-terminal end of CHMP2A (containing the following mutations: R16E, R27E, and K42) was amplified by PCR to create a mutant, N-terminal

CHMP2A PCR fragment. A C-terminal CHMP2A PCR fragment that contained the siRNA resistance mutations was also amplified by PCR. These N- and C-terminal PCR products were mixed with synthetic oligonucleotides that amplified full-length CHMP2A in a SOEing PCR reaction, resulting in full-length, mutant CHMP2A PCR product. This was then cloned into the pU6-CMV vector by AgeI/EcoRI restriction digest and ligation.

Cell lines

HeLa cells that stably expressed YFP-IST1 or YFP-IST1 3M were generated using an MuLV-based transduction system[56]. To create the transduction vector, the pQCXIN_YFP-IST1 or pQCXIN_YFP-IST1-3M (5 µg) expression vector was cotransfected into 293T cells (seeded at $2x10^6$ 24 h earlier) with the mammalian expression vector pGag-Pol (5 µg) and the VSV-G expression vector pMD.G (2 µg). The media was changed 12 h posttransfection. 36 h posttransfection, the vector-containing supernatant was collected in 1 ml aliquots, filtered (0.45 µm filter), frozen, and stored at −80º C.

HeLa cells to be transduced were seeded (initial density of ~$2x10^5$ cells/well) in a 6-well plate and incubated with a 1:1 mixture of 1 ml of vector-containing supernatant and 1ml fresh media for 12 h, followed by a media change and maintenance (1 week). The cells were maintained for approximately 1 week after which the YFP-positive cells were collected using the FACSAria Cell Sorter (University of Utah Cores), plated, allowed to grow for 2 weeks, harvested at 80% confluency, and frozen in conditioned media containing 10% DMSO and

52% FBS. Experiments involving YFP-IST1 or YFP-IST1-3M used cells from these frozen aliquots.

siRNA design and validation

siRNAs used in this study were: CGUACGCGGAAUACUUCGA (CON), $_{490}$AGAUACCUGAUUGAAAUUG$_{509}$ (IST1-1), and $_{377}$CCAAGUAUAGCAAG GAAUA$_{396}$ (IST1-2, numbers denote the target site in the sense strand of the coding region). The IST1-1 and CON (control) siRNAs had been validated and reported previously[25]. The IST1-2 siRNA was designed using the Dharmacon siDESIGN center (www.thermo.com/sidesign). The efficacy of IST1-2 siRNA mediated depletion of endogenous HeLa IST1 was validated using anti-IST1 immunoblots and immunofluorescence microscopy in fixed HeLa cells stained with anti-IST1 (Fig. 2.3, data not shown).

shRNA design, validation, and delivery and rescue

CHMP2A depletion studies used the following processed shRNAs: CGUACGCGGAAUACUUCGA (CON) and $_{395}$AGGCAGAGATCATGGATAT$_{412}$ (CHMP2A). This CHMP2A target site was used previously in siRNA depletion studies of CHMP2A, and the CON shRNA matches the CON siRNA listed above[56].

pU6-CMV vectors were used to create HIV-based transduction vectors to deliver shRNAs and express shRNA-resistant rescue constructs. These vectors were modified from the parent CSII-CMV-MCS vector (Riken BioResource

Center) by Devin Christiansen (Sundquist lab). In this vector, unprocessed RNA hairpins are expressed by RNA polymerase III from a U6 promoter. Rescue constructs are expressed from a downstream cytomegalovirus (CMV) promoter, and the mCherry transduction marker is expressed from a downstream internal ribosome entry site (IRES). Hence, these vectors express both the shRNA and the shRNA-resistant rescue construct, ensuring that all transduced cells depleted of CHMP2A will also express the exogenous rescue construct. When cotransfected with pCMVdeltaR8.91 (HIV Gag, Pol, and Rev) and (pMD.G VSV-G envelope) expression vectors, packageable proviral RNA expressed by the pU6-CMV is packaged into a pseudotyped HIV virus, creating a transduction vector.

siRNA transfections

HeLa cells (12- or 6-well plates) were transfected with duplex siRNA (final concentration of 20 nM) 24 h after seeding (initial density of $3x10^4$ or $2x10^5$ cells/well, respectively) using Lipofectamine RNAi MAX, following the manufacturer's recommendations. Cells were harvested for study 48 h posttransfection.

Antibody production, affinity purification, and sources

Polyclonal antibodies against IST1 and CHMP2A were raised against pure recombinant IST1 and CHMP2A in New Zealand White Rabbits (Covance,

Inc.)[25,56]. Anti-GAPDH (Millipore MAB374) and Anti-α̃tubulin (Sigma T6199) were both commercially available monoclonal antibodies.

The IST1 antibody was affinity purified to decrease background staining. Purified recombinant IST1 (10 µg) was immobilized on a sepharose column (GE Healthcare 17-0716-01) by amine coupling following manufacturer's recommendations. Antibody-containing serum was heat inactivated (30 min 56º C), diluted 1:5 in binding buffer (20 mM HEPES-buffered saline, pH 7.2), and applied to the column. The column was washed with 5–10 column volumes of binding buffer, and the protein was eluted with elution buffer (2% glycine, 150 mM NaCl, pH 3) and collected in 500 µl fractions directly into 500 µl aliquots of 2X antibody storage buffer (50 mM HEPES pH 7.2, 150 mM NaCl, and 3% BSA). Fractions containing the affinity-purified IST1 antibody were identified by immunoblotting against purified IST1.

Western blotting

HeLa cells (from single wells of a 6-well plate, $1x10^6$ cells/well) transfected with siRNA or transduced with shRNA were collected into 60 µl lysis buffer (50 mM HEPES pH 7.2, 150 mM NaCl, 1% triton X-100, 5 mM 2-mercaptoethanol, and a 1:200 dilution of mammalian protease inhibitor) and incubated on ice for 20 min to lyse the cells. The samples were diluted 1:1 into 2x SDS loading buffer (4% SDS, 0.1M Tris-HCL, 20% glycerol, 3.73 mM bromophenol blue, 5% 2-mercaptoethanol), and boiled for 5 min. Protein lysates were then electrophoresed (12.5% polyacrylamide) and transferred to PVDF membranes

(Millipore IPFL00010). Protein-containing PVDF membranes were incubated for 1 h in 5% milk in Tris-buffered saline (TBS; 135 mM NaCl, 2.5 mM KCl, 25 mM Tris base, pH 7.4) and then incubated overnight with primary antibody (1:500 affinity-purified IST1, 1:500 CHMP2A, or 1:10,000 GAPDH) diluted in 5% milk in TBS with .1% Tween (TBS-T). The membrane was then washed in TBS-T and incubated for 1 h with secondary antibodies diluted in 5% milk in TBS-T (1:10,000 IRDye 700DX, 611-730-127 VWR International and 1:10,000 Rockland IRDye 800, 610-132-121 VWR International). Membranes were washed again in TBS-T and visualized using the Odyssey Infrared Imaging System (LI-COR).

Immunofluorescence imaging

HeLa cell lines were seeded onto glass cover slips (12-well plates, $3X10^4$ cells/well) 24 h prior to siRNA transfection with siRNA transfection performed as described above. Forty-eight hours posttransfection, the cells were washed with PBS, incubated in 4% paraformaldehyde (37º C) or methanol (4º C) for 10 min, and washed twice more with PBS. These fixed cells were then incubated for 10–30 min in block/permeabilization buffer (BP buffer, PBS, 0.01% Triton X-100, 3% BSA).

Fixed, permeabilized cells were incubated for at least 2 h in primary antibody diluted in BP buffer (IST1 1:500; $\tilde{\alpha}$tubulin 1:10,000). Samples were washed twice with wash buffer (PBS, 0.01% Triton X-100), incubated in secondary antibody diluted in BP buffer for 1 h (1:1,000 Alexa Fluor 488, A21206 Invitrogen), and then incubated in SYTOX Green (Invitrogen S7020; 1 µM in

wash buffer) or Hoechst (Invitrogen H21492, 1 μM in wash buffer) to stain the nuclei (10 min 23ºC). The fixed and stained cells were washed twice more with wash buffer, and the cover slips were mounted on slides and visualized in Fluoromount G mount solution (Fisher Scientific 0100-01).

Fluorescence microscopic quantification of abscission failure

Cells were prepared for immunofluorescence as described above and the fraction of cells with visible intercellular bridges or multiple nuclei was quantified (cells with visible intercellular bridges or multiple nuclei divided by total cells counted). The increase in the fraction of cells with visible intercellular bridges or multiple nuclei as compared to control was defined as the fraction of cells that failed in abscission. Three groups of 100 cells were counted and averaged to obtain error bars for each experiment, and the entire experiment was repeated three times.

DNA content assays for abscission failure

Abscission failure was also scored by analyzing the DNA contents of HeLa cells transduced with the pU6-CMV vectors (pU6.CON-CMV, pU6.CHMP2A-CMV, pU6.CON-CMV.CHMP2A, pU6.CHMP2A-CMV.CHMP2A, pU6.CON-CMV.CHMP2A3M, and pU6.CHMP2A-CMV.CHMP2A3M). Each pU6-CMV expression vector (5 μg) was cotransfected (PEI) into 293T cells (24 h after seeding, initial density of $2x10^6$ in a 10 cm dish) together with the pCMVdeltaR8.91 (5 μg) and pMD.G (2 μg) vectors. The media was changed 12

h posttransfection. The virus-containing supernatant was collected 36 h posttransfection, filtered (.45 μm filter), frozen, and stored at −80º C in 1 ml aliquots.

HeLa cells were seeded (initial density of $2x10^5$ cells/well) in 6-well plates and transduced with 1:1 mixture of 1 ml of virus-containing supernatant from the frozen stock and 1ml of fresh media. The media was changed 12 h posttransduction, and the cells were reseeded 48 h posttransduction into 6-well plates (initial density of $4x10^5$ cells/well).

After an additional 48 h, cells from each well were individually treated with trypsin, washed, and incubated in 0.4 ml of propidium iodide solution (50 μg/ml of propidium iodide, in PBS, 0.01% Triton X-100, .25 mg RNase/ml, at 4ºC for 30 min). 10^4 cells were analyzed for propidium iodide fluorescence using the FACScanII flow cytometer, and peak volumes were analyzed using Modfit LT software (version 2.0) to determine the percentage of cells with 2C, 4C, and 8C DNA contents. An increase in the percent of cells with 4C and 8C DNA contents as compared to control is the fraction of cells that failed in abscission.

Results and Discussion

IST1 depletion/rescue assay

The IST1 depletion/rescue assay was validated by showing that: 1) depletion of endogenous IST1 resulted in an increase of the fraction of cells with visible intercellular bridges or multiple nuclei and 2) expression of exogenous, wild-type IST1 from an siRNA-resistant construct rescued the increase of the fraction of cells with visible intercellular bridges or multiple nuclei in cells depleted

of endogenous IST1. The fraction of cells with a visible intercellular bridge or multiple nuclei induced by IST1 was quantified by determining the fraction of cells that exhibited either visible intercellular bridges or multiple nuclei (Fig. 2.3).

Treatment of HeLa cells with either of two siRNAs that targeted IST1 (termed IST1-1 and IST1-2) efficiently depleted endogenous IST1 from HeLa cells as measured by western blotting (Fig. 2.3, panel 2, compare lanes 2 and 3 to lane 1). In both cases, IST1 depletion resulted in the fraction of cells with visible intercellular bridges or multiple nuclei (31% ± 4% and 36% ± 1%, respectively) as compared to HeLa cells treated with a control siRNA (9% ± 0,8%, CON, Fig. 2.3, panel 1, compare lanes 2 and 3 to lane 1). Thus, IST1 depletion induces a measurable phenotype.

The fraction of cells with visible intercellular bridges or multiple nuclei was normal in a HeLa cell line depleted of endogenous IST1 and expressing siRNA-resistant YFP-IST1, demonstrating that exogenous expressed IST1 can functionally replace the endogenous protein. To perform these experiments, I created a stable HeLa cell line expressing an siRNA-resistant YFP-IST1 construct. As shown in Fig. 2.3, these cells expressed both endogenous IST1 and YFP-IST1, as assayed by western blotting with an anti-IST1 antibody (Fig. 2.3, panel 2, lane 4). Expression of the YFP-IST1 protein did not increase the fraction of cells with visible intercellular bridges or multiple nuclei (Fig. 2.3, panel 1, compare lanes 1 and 4, 9% ± 0.8% and 9% ± 3%, respectively). As expected, treatment with IST-1 siRNA depleted the endogenous IST1 protein but did not affect the levels of the siRNA-resistant YFP-IST1 construct (Fig. 2.3, panel 2,

compare lanes 4 and 5). Importantly, this treatment did not significantly increase the fraction of cells with visible intercellular bridges or multiple nuclei as compared to treatment with a control siRNA (Fig. 2.3, panel 1, compare lanes 1 and 5, 9% ± 3% and 11% ± 1%, respectively). As expected, however, treatment with IST1-2 siRNA depleted both endogenous IST1 and exogenous YFP-IST1 and induced a dramatic increase in the fraction of cells with visible intercellular bridges or multiple nuclei (Fig. 2.3, panel 1, compare lanes 1 and 6, 9% ± 3% and 41% ± 0.4%, respectively). I therefore conclude that the increase in the fraction of cells with visible intercellular bridges or multiple nuclei induced by treatment with either of the IST1 siRNAs is specifically caused by IST1 depletion and that the siRNA-resistant YFP-IST1 constructs can rescue the increase in the fraction of cells with visible intercellular bridges or multiple nuclei induced by depletion of endogenous IST1.

CHMP2A depletion/rescue assay

As with the IST1 depletion/rescue assay, the CHMP2A depletion/rescue assay was validated by showing that: 1) depletion of endogenous CHMP2A resulted in an increase in the fraction of cells with 4 and 8C DNA contents and 2) wild-type CHMP2A from an shRNA-resistant construct rescued the increase in the fraction of cells with 4 and 8C DNA contents in cells depleted of CHMP2A. In this assay, the percentage of cells with 4 and 8C DNA contents were quantified using DNA content analyses (Fig. 2.4).

Treatment of HeLa cells with a CHMP2A shRNA depleted endogenous

CHMP2A as determined by western blotting (Fig. 2.4, panel 2, lane 2). CHMP2A depletion induced an increase in the fraction of cells with 4 and 8C DNA contents as compared to HeLa cells treated with a control shRNA (CON; Fig. 2.4, panel 1, compare lanes 1 and 2, 14% ± 0.5% 4C, 0.5% ± 0.2% 8C vs. 22% ± 4% 4C, 6% ± 2% 8C, respectively). Hence, CHMP2A depletion significantly increases the fraction of cells with 4 and 8C DNA contents, producing a measurable phenotype.

The fraction of cells with 4 and 8C DNA contents was normal in HeLa cells depleted of endogenous CHMP2A and expressing shRNA-resistant CHMP2A, demonstrating that exogenous CHMP2A can functionally replace endogenous protein. To perform these experiments, I created transduction vectors that expressed a CHMP2A or control (CON) shRNA and an shRNA-resistant CHMP2A construct (pU6.CHMP2A_CMV_CHMP2A and pU6.CON_CMV .CHMP2A). As shown in Fig. 2.4, HeLa cells expressing both endogenous and exogenous CHMP2A did not show an increase in the fraction of cells with 4 and 8C DNA contents (compare lanes 1 and 3, 14% ± 0.5% 4C, 0.5% ± 0.2% 8C vs. 13% ± 2% 4C, .8% ± 0.4% 8C, respectively). Importantly, HeLa cells expressing exogenous CHMP2A and depleted of endogenous protein also had a normal fraction of cells with 4 and 8C DNA contents (Fig. 2.4, compare lanes 1 and 4, 14% ± 0.4% 4C, 0.7% ± 0.2% 8C vs. 12% ± 1% 4C, 0.7% ± 0.2% 8C, respectively). These data confirm that CHMP2A depletion induces an increase in the fraction of cells with 4 and 8C DNA contents and that exogenous CHMP2A can functionally replace the endogenous protein.

Functional importance of the basic patch on ESCRT-III helix one

The IST1 and CHMP2A depletion/rescue assays were used to test the model for membrane binding proposed by Weissenhorn and colleagues, and to provide a "proof of principle" that these assays could be used in genetic analyses of IST1 and CHMP2A abscission functions[24]. The model for ESCRT-III membrane binding proposed by Weissenhorn and colleagues predicts that the exposed basic patches on the first alpha helix of IST1 and CHMP2A mediate membrane binding[24]. To test this model, I generated siRNA-resistant expression constructs with the following basic-patch mutations: YFP-IST1 3M (containing the helix one basic patch mutations R16E, R27E, and K38E) and CHMP2A 3M (containing the helix one basic patch mutations R16E, R27E, and K42E). As illustrated in Fig. 2.5, these charge reversals eliminated the basic character of the helix one patches, and were therefore expected to abrogate any ionic membrane interactions mediated by these patches. The mutant ESCRT-III protein IST1 lacking the basic patches failed to function in abscission while the mutant CHMP2A protein function in abscission was ambiguous, demonstrating the importance of this patch for IST1 function in abscission.

To test the functionality of the mutant YFP-IST1 3M protein, I generated a HeLa cell line that expressed this protein at approximately the same level as the wild-type YFP-IST1 control line (Fig. 2.3, panel 2, compare lanes 4 and 7). This cell line did not show an increase in the fraction of cells with visible intercellular bridges or multiple nuclei, demonstrating that the mutant YFP-IST1 3M protein did not dominantly inhibit endogenous IST1 protein function (panel 1, compare

lane 7 to lanes 4 and 1; 8% ± 1%, 9% ± 3%, and 9% ± 0.8%, respectively). However, depletion of endogenous IST1 with the IST1-1 siRNA resulted in a dramatic increase in the fraction of cells with visible intercellular bridges or multiple nuclei (Fig. 2.3, lane 8, 39% ± 6%). This treatment did not alter exogenous YFP-IST1 3M protein levels, and I therefore conclude that, unlike wild-type IST1, the mutant YFP-IST1 3M protein cannot rescue the increase in the fraction of cells with visible intercellular bridges or multiple nuclei induced by depletion of endogenous IST1. As expected, treatment with IST1-2 siRNA depleted both endogenous IST1 and exogenous YFP-IST1 3M, resulting in an even greater increase in the fraction of cells with visible intercellular bridges or multiple nuclei (Fig. 2.3, lane 9, 40% ± 1%).

To determine the functionality of the CHMP2A 3M protein, I created transduction vectors that expressed control shRNA (CON) or an shRNA that targeted CHMP2A, as well as an shRNA-resistant CHMP2A 3M construct. As shown in Fig. 2.4, HeLa cell expression of CHMP2A 3M did not cause and increase in the fraction of cells with 4 and 8C DNA contents (compare lane 1 to lane 5, 14% ± 0.5% 4C, 0.5% ± 0.2% 8C, vs. 14% ± 2% 4C, 0.5% ± 0.1% 8C, respectively). However, HeLa cells that expressed CHMP2A 3M and were depleted of endogenous CHMP2A exhibited a significant increase in the fraction of cells with 4 and 8C DNA contents (Fig. 2.4, compare lane 1 to lane 6, 14% ± 0.5% 4C, 0.5% ± 0.2% 8C vs. 18% ± 1% 4C, 3% ± 0.9% 8C, respectively).

Summary

In summary, I have developed and validated IST1 and CHMP2A depletion/rescue assays and shown that these assays can be used in genetic analyses of IST1 and CHMP2A function in abscission. My data also confirm the functional importance of the basic patches on helix one of IST1 consistent with the ESCRT-III membrane-binding model proposed by Weissenhorn and colleagues; however, these experiments did not specifically implicate these residues in membrane binding[24]. My attempts to confirm the importance of the basic patches of IST1 in membrane were inconclusive. Mutant IST1 protein lacking the basic patches failed to localize to the intercellular bridge, suggesting that these mutations produced a transport/localization defect (data not shown). The functional importance of the CHMP2A basic patches is also ambiguous in the present work. The ability of CHMP2A 3M to functionally replace endogenous protein was dependent upon viral titer used in the transduction, where high viral titers indicated that CHMP2A 3M partially functionally replaced endogenous protein, and low viral titers suggested that CHMP2A 3M did not functionally replace endogenous protein (data from all titers were included in Fig. 2.4). Possible reasons for this include mutation of nonessential basic residues or mutation of too few basic residues in CHMP2A 3M. Importantly, this phenomenon was unique to the CHMP2A 3M construct as all other constructs showed no differences due to viral titer.

In the future, these assays can be applied to address other aspects of IST1 and CHMP2A functions in abscission. Important questions in this regard

include defining the protein:protein interactions that support IST1 and CHMP2A filament formation and analyzing the features that allow these filaments to form tapering cones and mediate membrane juxtaposition and fission of the intercellular bridge.

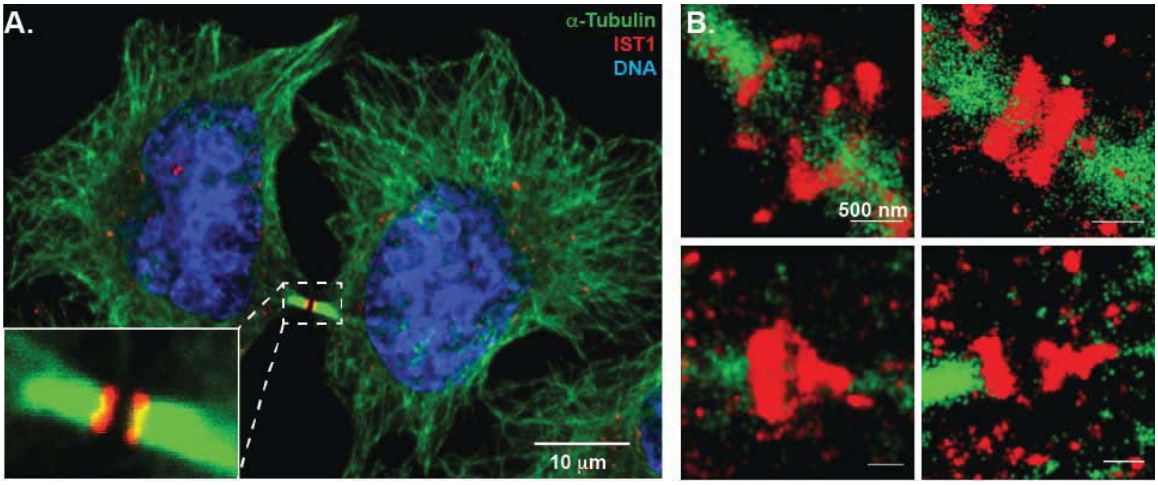

Figure 2.1: IST1 forms rings and cones within the intercellular bridge *(images provided by Leremy Colf).* (A) IST1 localizes to the intercellular bridge. Confocal fluorescence microscopic image of two nascent daughter cells connected by an intercellular bridge (boxed). α-tubulin is stained green, IST1 is stained red, and DNA is stained blue. (B) D-storm super-resolution fluorescence microscopic images showing that IST1 forms rings (top two panels) and cones (bottom two panels) within the intercellular bridge. α-tubulin is stained green and IST1 is stained red.

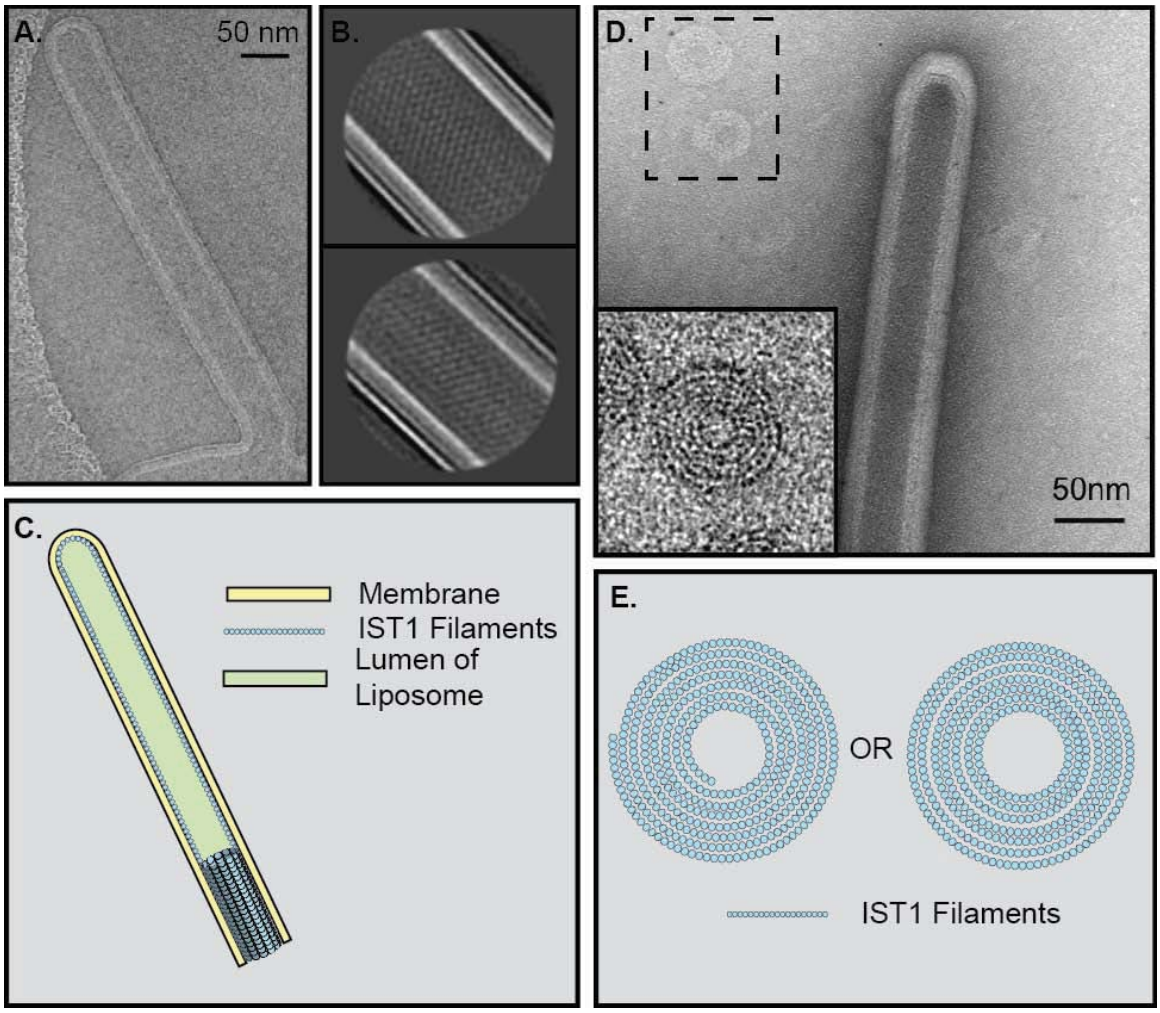

Figure 2.2: Purified IST1$_{NTD}$ forms helices that can deform liposomes from within the lumen and can also form spiraling filaments or concentric rings *(images provided by John McCullough and Adam Frost).* (A) Cryo-electron microscopic image of IST1:lipid tubes extruding from the lumen of a liposome. Note that the IST1 helices bind to the inner leaflet of the liposome bilayer. (B) 2-D class averages of helical IST1:lipid tubes, demonstrating that IST1 forms a lattice on the lumenal side of the lipid bilayer. (C) Image representing IST1:lipid tubes showing helical IST1 filaments. Note that the IST1 helix shown at the bottom of the tube extends the length of the tube (not shown). (D) Negatively stained electron microscopic image of an IST1:lipid tube and adjacent IST1 assemblies. Inset: low-pass filtered, local contrast-enhanced image of IST1 filaments forming concentric rings or spirals. (E) Image representing IST1 filaments forming concentric rings or spirals.

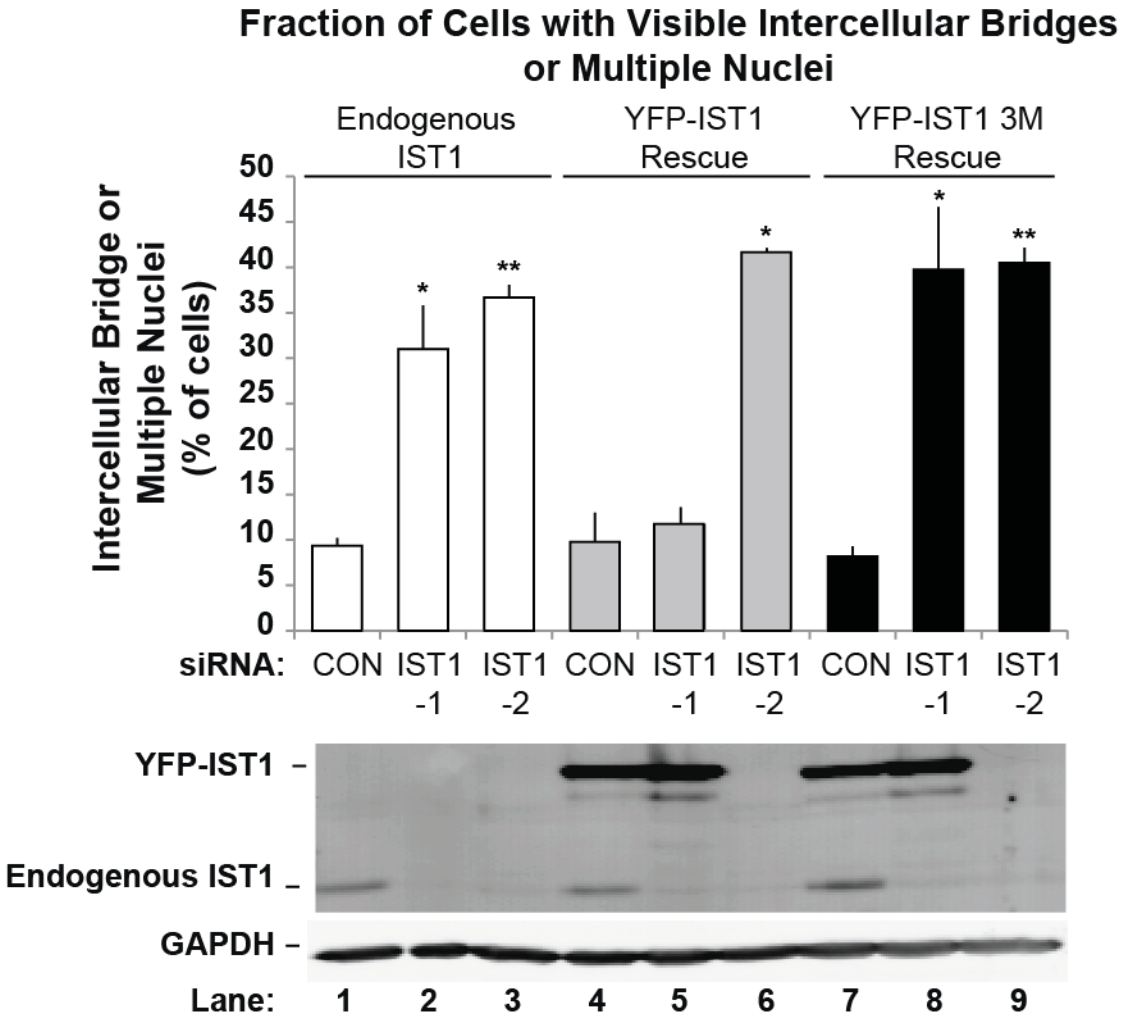

Figure 2.3: IST1 is required for HeLa cell abscission, and IST1 function(s) require basic residues of the N-terminal helix. Panel 1 shows the percentage of cells in each sample with abscission defects. Error bars show standard deviations from four experiments except in lanes 3, 6, and 9 in which the error bar represents a range from two experiments. P-values less than .005 (*), and less than .0005 (**) are indicated (compared to the each cell type control). The HeLa cell type being tested is indicated above the appropriate columns in the graph. Samples were treated with the siRNA listed directly below the x-axis. Panel 2 is a representative western blot (anti-IST1) showing the levels of endogenous IST1 and exogenous YFP-IST1 protein in each sample. Panel 3 (anti-GAPDH) shows the levels of the GAPDH loading control in each sample.

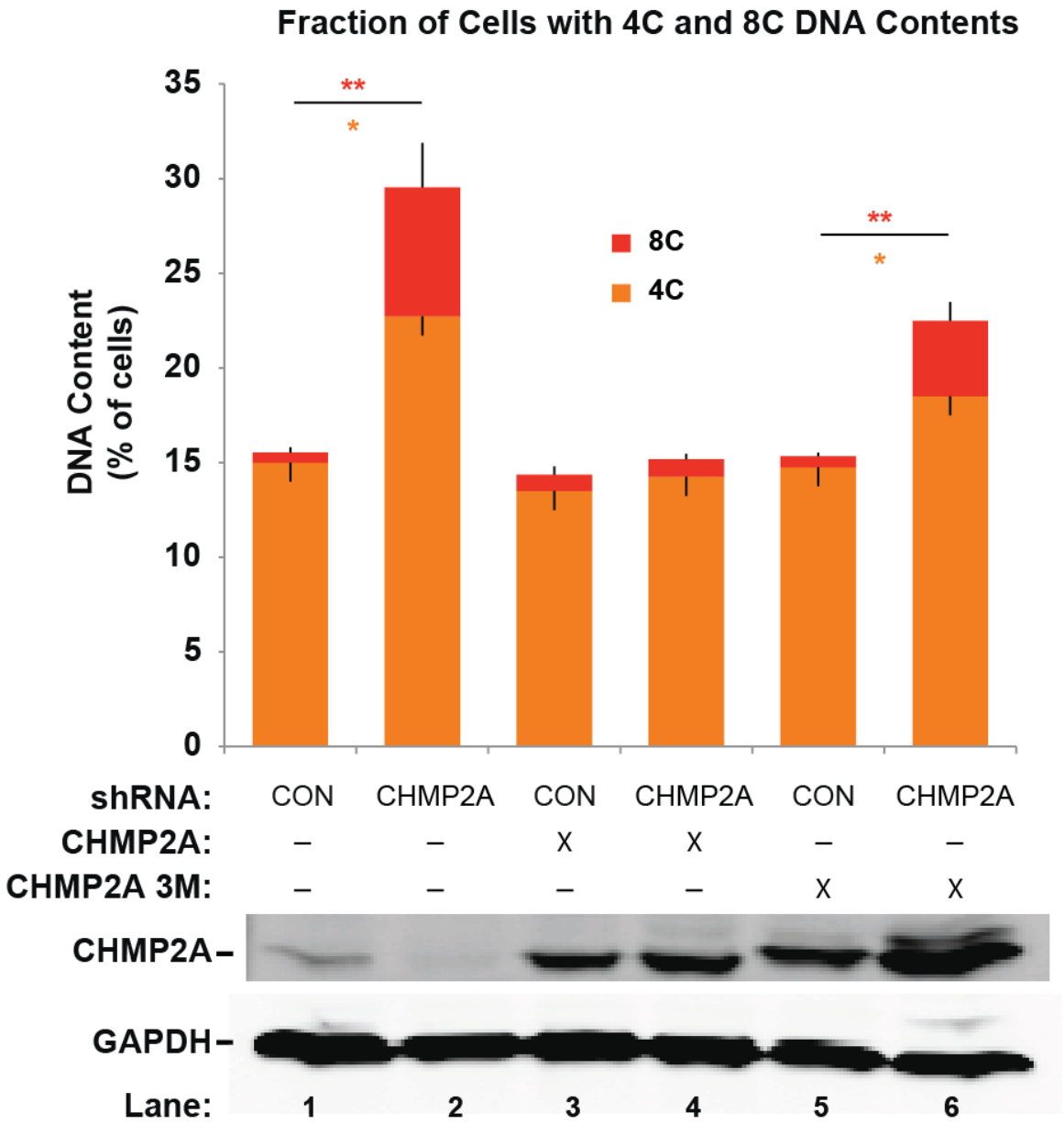

Figure 2.4: CHMP2A is required for HeLa cell abscission, and CHMP2A function(s) requires the basic residues of the N-terminal helix. Panel 1 shows the percentages of cells with 4C (orange) and 8C (red) DNA content (a measure of abscission failure). Error bars show standard deviations calculated from six experiments. P-values less than .005 (*) and less than .0005 (**) are indicated. The shRNA and exogenous, shRNA-resistant protein expressed in each sample are listed below the x-axis. Panel 2 is a representative western blot (anti-CHMP2A) showing protein levels in each sample. Panel 3 is a western blot (anti-GAPDH) showing levels of the GAPDH loading control in each sample.

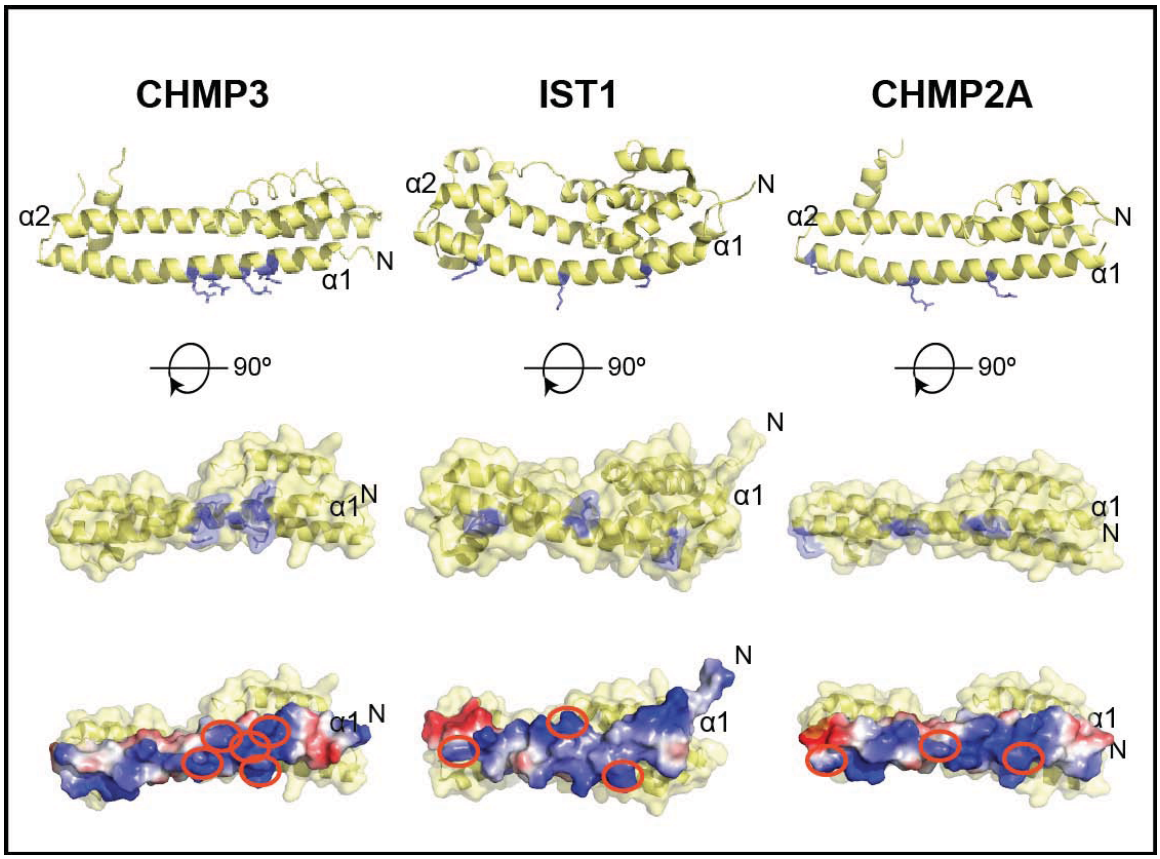

Figure 2.5: Putative membrane binding surfaces of CHMP3, IST1, and CHMP2A. The figure shows ribbon diagrams (row 1), space-filling models (row 2), and electrostatic maps of the helix 1 surface (row 3), with basic regions in blue, acidic regions in red, and neutral regions in white. Basic residues that were mutated to make the CHMP3 5M, IST 3M, and CHMP2A 3M constructs are colored blue in rows 1 and 2, and circled in red in row 3[24]. Helix 1 is located at the bottom of the structures in row 1, and oriented toward the viewer in rows 2 and 3. The PDB numbers for the structures used are: 2DG5 (CHMP3) and 3FRR (IST1). A CHMP2A homology model was created using the PHYRE protein fold recognition server (http://www.sbg .bio.ic.ac.uk/~phyre/, *provided by Heidi Schubert*).

Table 2.1: Plasmids used in this study.

Plasmid Name	Internal Plasmid ID
pGag-Pol	WISP 07-127
pMD.G	WISP 03-279
pCMVdeltaR8.91	WISP 06-72
pCDNA_IST1 (siResistant 490)	WISP 08-33
pCMV_CHMP2A (siResistant 395, 464)	WISP 12-103
pQCXIN_YFP-IST1	WISP 13-89
pQCXIN_YFP-IST1-3M	WISP 13-123
pU6.CON-CMV	WISP 13-124
pU6.CHMP2A-CMV	WISP 13-125
pU6.CON-CMV.CHMP2A	WISP 12-162
pU6.CHMP2A-CMV.CHMP2A	WISP 12-163
pU6.CON-CMV.CHMP2A3M	WISP 13-126
pU6.CHMP2A-CMV.CHMP2A3M	WISP 13-127

LITERATURE CITED

1. Bryant, N. J. & Stevens, T. H. Vacuole biogenesis in Saccharomyces cerevisiae: protein transport pathways to the yeast vacuole. *Microbiol. Mol. Biol. Rev.* **62**, 230–247 (1998).

2. McCullough, J., Colf, L. A. & Sundquist, W. I. Membrane fission reactions of the mammalian ESCRT pathway. *Annu. Rev. Biochem.* **82**, 663–692 (2012).

3. Martin-Serrano, J. & Neil, S. J. D. Host factors involved in retroviral budding and release. *Nat. Rev. Microbiol.* **9**, 519–531 (2011).

4. Weiss, E. R. & Göttlinger, H. The role of cellular factors in promoting HIV budding. *J. Mol. Biol.* **410**, 525–533 (2011).

5. Doherty, G. J. & McMahon, H. T. Mechanisms of endocytosis. *Annu. Rev. Biochem.* **78**, 857–902 (2009).

6. Campelo, F. & Malhotra, V. Membrane fission: the biogenesis of transport carriers. *Annu. Rev. Biochem.* **81**, 407–427 (2012).

7. Banta, L. M., Robinson, J. S., Klionsky, D. J. & Emr, S. D. Organelle assembly in yeast: characterization of yeast mutants defective in vacuolar biogenesis and protein sorting. *J. Cell Biol.* **107**, 1369–1383 (1988).

8. Raymond, C. K., Howald-Stevenson, I., Vater, C. A. & Stevens, T. H. Morphological classification of the yeast vacuolar protein sorting mutants: evidence for a prevacuolar compartment in class E vps mutants. *Mol. Biol. Cell* **3**, 1389–1402 (1992).

9. Katzmann, D., Babst, M. & Emr, S. Ubiquitin-dependent sorting into the multivesicular body pathway requires the function of a conserved endosomal protein sorting complex, ESCRT-I. *Cell, **106**, 145–155* (2001).

10. Babst, M., Sato, T. K., Banta, L. M. & Emr, S. D. Endosomal transport function in yeast requires a novel AAA-type ATPase, Vps4p. *EMBO J.* **16**, 1820–1831 (1997).

11. Babst, M., Katzmann, D. J., Snyder, W. B., Wendland, B. & Emr, S. D. Endosome-associated complex, ESCRT-II, recruits transport machinery for protein sorting at the multivesicular body. *Dev. Cell* **3**, 283–289 (2002).

12. Babst, M., Katzmann, D. J., Estepa-Sabal, E. J., Meerloo, T. & Emr, S. D. Escrt-III: an endosome-associated heterooligomeric protein complex required for mvb sorting. *Dev. Cell* **3**, 271–282 (2002).

13. Raiborg, C. & Stenmark, H. Hrs and endocytic sorting of ubiquitinated

membrane proteins. *Cell Struct. Funct.* **27**, 403–408 (2002).

14. Nabhan, J. F., Hu, R., Oh, R. S., Cohen, S. N. & Lu, Q. Formation and release of arrestin domain-containing protein 1-mediated microvesicles (ARMMs) at plasma membrane by recruitment of TSG101 protein. *Proc. Natl. Acad. Sci.* **109**, 4146–4151 (2012).

15. Rauch, S. & Martin-Serrano, J. Multiple interactions between the ESCRT machinery and arrestin-related proteins: implications for PPXY-dependent budding. *J. Virol.* **85**, 3546–3556 (2011).

16. Lin, C. H., MacGurn, J. A., Chu, T., Stefan, C. J. & Emr, S. D. Arrestin-related ubiquitin-ligase adaptors regulate endocytosis and protein turnover at the cell surface. *Cell* **135**, 714–725 (2008).

17. Carlton, J. G. & Martin-Serrano, J. Parallels between cytokinesis and retroviral budding: a role for the ESCRT machinery. *Science* **316**, 1908–1912 (2007).

18. Lee, H. H., Elia, N., Ghirlando, R., Lippincott-Schwartz, J. & Hurley, J. H. Midbody targeting of the ESCRT machinery by a noncanonical coiled coil in CEP55. *Science* **322**, 576–580 (2008).

19. Zhao, W.-M., Seki, A. & Fang, G. Cep55, a microtubule-bundling protein, associates with centralspindlin to control the midbody integrity and cell abscission during cytokinesis. *Mol. Biol. Cell* **17**, 3881–3896 (2006).

20. Sundquist, W. I. & Krausslich, H. G. HIV-1 Assembly, budding, and maturation. *Cold Spring Harb. Perspect. Med.* **2**, a006924–a006924 (2012).

21. Xiao, J. *et al.* Structural basis of Ist1 function and Ist1-Did2 interaction in the multivesicular body pathway and cytokinesis. *Mol. Biol. Cell* **20**, 3514–3524 (2009).

22. Dimaano, C., Jones, C. B., Hanono, A., Curtiss, M. & Babst, M. Ist1 regulates Vps4 localization and assembly. *Mol. Biol. Cell* **19**, 465–474 (2008).

23. Bajorek, M. *et al.* Structural basis for ESCRT-III protein autoinhibition. *Nat. Struct. Mol. Biol.* **16**, 754–762 (2009).

24. Muzioł, T. *et al.* Structural basis for budding by the ESCRT-III factor CHMP3. *Dev. Cell* **10**, 821–830 (2006).

25. Bajorek, M. *et al.* Biochemical analyses of human IST1 and its function in cytokinesis. *Mol. Biol. Cell* **20**, 1360–1373 (2009).

26. Im, Y. J., Wollert, T., Boura, E. & Hurley, J. H. Structure and function of the ESCRT-II-III interface in multivesicular body biogenesis. *Dev. Cell* **17**, 234–243 (2009).

27. Yorikawa, C. *et al.* Human CHMP6, a myristoylated ESCRT-III protein, interacts directly with an ESCRT-II component EAP20 and regulates endosomal cargo sorting. *Biochem. J.* **387**, 17–26 (2005).

28. Teo, H., Perisic, O., González, B. & Williams, R. L. ESCRT-II, an endosome-associated complex required for protein sorting: crystal structure and interactions with ESCRT-III and membranes. *Dev. Cell* **7**, 559–569 (2004).

29. Langelier, C. *et al.* Human ESCRT-II complex and its role in human immunodeficiency virus type 1 release. *J. Virol.* **80**, 9465–9480 (2006).

30. McCullough, J., Fisher, R. D., Whitby, F. G., Sundquist, W. I. & Hill, C. P. ALIX-CHMP4 interactions in the human ESCRT pathway. *Proc. Natl. Acad. Sci.* **105**, 7687–7691 (2008).

31. Mu, R. *et al.* Two distinct binding modes define the interaction of Brox with the C-terminal tails of CHMP5 and CHMP4B. *Structure* **20**, 887–898 (2012).

32. Lata, S. *et al.* Helical structures of ESCRT-III are disassembled by VPS4. *Science* **321**, 1354–1357 (2008).

33. Effantin, G. *et al.* ESCRT-III CHMP2A and CHMP3 form variable helical polymers in vitro and act synergistically during HIV-1 budding. *Cell. Microbiol.* **15**, 213–226 (2013).

34. Hanson, P. I., Roth, R., Lin, Y. & Heuser, J. E. Plasma membrane deformation by circular arrays of ESCRT-III protein filaments. (2008).

35. Guizetti, J. *et al.* Cortical constriction during abscission involves helices of ESCRT-III-dependent filaments. *Science* **331**, 1616–1620 (2011).

36. Stuchell-Brereton, M. D. *et al.* ESCRT-III recognition by VPS4 ATPases. *Nature* **449**, 740–744 (2007).

37. Kieffer, C., Skalicky, J., Morita, E. & De Domenico, I. Two distinct modes of ESCRT-III recognition are required for VPS4 functions in lysosomal protein targeting and HIV-1 budding. *Dev. Cell* (2008).

38. Obita, T. *et al.* Structural basis for selective recognition of ESCRT-III by the AAA ATPase Vps4. *Nature* **449**, 735–739 (2007).

39. Hill, C. P. & Babst, M. Structure and function of the membrane deformation AAA ATPase Vps4. *Biochim. Biophys. Acta* **1823**, 172–181 (2012).

40. Jouvenet, N., Zhadina, M., Bieniasz, P. D. & Simon, S. M. Dynamics of ESCRT protein recruitment during retroviral assembly. *Nat. Cell Biol.* **13**, 394–401 (2011).

41. Baumgärtel, V. *et al.* Live-cell visualization of dynamics of HIV budding site interactions with an ESCRT component. *Nat. Cell Biol.* **13**, 469–474 (2011).

42. Elia, N., Fabrikant, G., Kozlov, M. M. & Lippincott-Schwartz, J. Computational model of cytokinetic abscission driven by ESCRT-III polymerization and remodeling. *Biophys. J.* **102**, 2309–2320 (2012).

43. Fabrikant, G. *et al.* Computational model of membrane fission catalyzed by ESCRT-III. *PLoS Comput. Biol.* **5**, e1000575 (2009).

44. Elia, N., Sougrat, R., Spurlin, T. A., Hurley, J. H. & Lippincott-Schwartz, J. Dynamics of endosomal sorting complex required for transport (ESCRT) machinery during cytokinesis and its role in abscission. *Proc. Natl. Acad. Sci.* **108**, 4846–4851 (2011).

45. Boura, E. *et al.* Solution structure of the ESCRT-I and -II supercomplex: implications for membrane budding and scission. *Structure* **20**, 874–886 (2012).

46. Morita, E. *et al.* Human ESCRT and ALIX proteins interact with proteins of the midbody and function in cytokinesis. *EMBO J.* **26**, 4215–4227 (2007).

47. Agromayor, M. & Martin-Serrano, J. Knowing when to cut and run: mechanisms that control cytokinetic abscission. *Trends Cell Biol.* **23**, 433–441 (2013).

48. Somers, W. G. & Saint, R. A RhoGEF and Rho Family GTPase-activating protein complex links the contractile ring to cortical microtubules at the onset of cytokinesis. *Dev. Cell* **4**, 29–39 (2003).

49. Glotzer, M. Animal cell cytokinesis. *Annu. Rev. Cell Dev. Biol.* **17**, 351–386 (2001).

50. Eggert, U. S., Mitchison, T. J. & Field, C. M. Animal cytokinesis: from parts list to mechanisms. *Annu. Rev. Biochem.* **75**, 543–566 (2006).

51. Glotzer, M. M. The 3Ms of central spindle assembly: microtubules, motors and MAPs. *Nat. Rev. Mol. Cell Biol.* **10**, 9–20 (2009).

52. Kim, J. *et al.* Structural basis for endosomal targeting by the Bro1 domain. *Dev. Cell* **8**, 937–947 (2005).

53. Bissig, C. *et al.* Viral infection controlled by a calcium-dependent lipid-binding module in ALIX. *Dev. Cell* **25**, 364–373 (2013).

54. Pineda-Molina, E. *et al.* The crystal structure of the C-terminal domain of Vps28 reveals a conserved surface required for Vps20 recruitment. *Traffic* **7**, 1007–1016 (2006).

55. Teo, H. *et al.* ESCRT-I core and ESCRT-II GLUE domain structures reveal role for GLUE in linking to ESCRT-I and membranes. *Cell* **125**, 99–111 (2006).

56. Morita, E. *et al.* Human ESCRT-III and VPS4 proteins are required for centrosome and spindle maintenance. *Proc. Natl. Acad. Sci.* **107**, 12889–12894 (2010).

57. Agromayor, M. *et al.* Essential role of hIST1 in cytokinesis. *Mol. Biol. Cell* **20**, 1374–1387 (2009).

58. Garrus, J. E. *et al.* Tsg101 and the vacuolar protein sorting pathway are essential for HIV-1 budding. *Cell* **107**, 55–65 (2001).

59. Ghazi-Tabatabai, S. *et al.* Structure and disassembly of filaments formed by the ESCRT-III subunit Vps24. *Structure* **16**, 1345–1356 (2008).

60. Pires, R. *et al.* A crescent-shaped ALIX dimer targets ESCRT-III CHMP4 filaments. *Structure* **17**, 843–856 (2009).

61. Bodon, G. *et al.* Charged multivesicular body protein 2B (CHMP2B) of the endosomal sorting complex required for transport-III (ESCRT-III) polymerizes into helical structures deforming the plasma membrane. *J. Biol. Chem.* **286**, 40276–40286 (2011).